A technique for the measurement of the plane wave reflection coefficient of shallow water seabeds

P. F. Joseph

Institute of Sound and Vibration Research, University of Southampton, Highfield, Southampton SO45 3BL, UK.
pfj@isvr.soton.ac.uk

Abstract

This paper presents a two–part measurement technique for determining the complex plane wave reflection coefficient at the seabed of iso-speed, and nearly iso-speed shallow water channels. The first procedure allows for the measurement of the reflection loss, while the second, the reflection phase. Each technique may be implemented independently of each other.

1. Introduction

Existing techniques for measuring shallow water seabed reflection coefficients divide into two categories. The first type attempt, either to 'gate out' the reflections following the first bottom interaction, or try to deduce the angle of incidence at the seabed from the time of arrival of short duration signals. The limits on the frequency and angular resolution on the reflection coefficient measurement imposed by this restriction is generally unacceptable in very shallow water or at low frequencies. A good review of this type of measurement is presented by Schmidt and Jensen [1]. The second type of approach, of which there are far fewer examples in the literature, allows for the steady state, multiple reflections between the boundaries by incorporating their influence into the processing algorithms. Their disadvantage, however, is that the reflection coefficient appears as a highly non-linear function of the measured acoustic pressure whose solution from these measurements is therefore difficult. An elegant example of the second type of approach is presented by Frisk *et al.* [2]. This method uses the Hankel transform of the acoustic pressure measured as a function of range to obtain an estimate for the Green function wavenumber spectrum. By equating this measurement to the theoretical Green function, the seabed reflection coefficient can, in principle, be determined directly. In the special case of an iso-speed waveguide the reflection coefficient bears a simple closed form, algebraic relationship to the measured Green function. This technique has also been proposed by Lambert *et al.* [3]. However, Cox and Joseph [4] have recently shown through computer simulations that, in general, the accuracy of the Green function measurement necessary to implement this procedure, particularly its phase, is generally greater than that usually achievable in real ocean environments. Much of the problem is shown to arise, not only from the inherent ill-conditioning of the inversion procedure, but from the fundamental limitations of the Hankel Transform routines themselves. Another example of the second type of technique is proposed by Yang and Yates [5] based upon full field inversion techniques. Unlike the approach proposed here, it relies on the user to make an initial guess of the complex plane reflection coefficient. The solution is then obtained though successive perturbations to this guess until an optimal match is achieved to the beam intensities measured by a Vertical Line Array of hydrophone sensors. The present paper describes a measurement technique for determining the complex plane wave reflection coefficient of horizontally stratified seabeds in iso-speed, and nearly iso-speed, shallow water waveguides. The technique uses acoustic pressure measurements made by a Vertical Line Array (VLA) of receiver hydrophones and a single towable sound source

2. Basic Relationships

The spatial variation of the acoustic pressure $p(r,z)$ due to a point source at $(0, z_0)$ in a horizontally stratified shallow water waveguide of depth H bounded by upper and lower impedance boundaries with plane wave reflection coefficients $S(\gamma)$ and $R(\gamma)$ respectively, at a single frequency ω is given by [6],

$$\left[\frac{1}{r}\frac{\partial}{\partial r}\left(r\frac{\partial}{\partial r}\right)+\frac{\partial^2}{\partial z^2}+k^2(z)\right]p(r,z)=-2\frac{\delta(r)}{r}\delta(z-z_0), \qquad (1)$$

where γ is the vertical wavenumber component of sound in water, $k(z)=\omega/c(z)$, ω is the angular frequency, $c(z)$ is the depth dependent sound speed variation and δ is the Dirac delta function. The solution for $p(r,z)$ may be expressed as a zero order Hankel Transform of the depth dependent Green function $g(z,z_0;\gamma)$ which form the transform pair:

$$p(r,z)=\int_0^\infty g(z_0,z;\gamma)J_0(k_r r)k_r dk_r\,,\quad g(z,z_0;\gamma)=\int_0^\infty p(r,z)J_0(k_r r)rdr\,, \qquad (2,3)$$

TG Leighton, GJ Heald, HD Griffiths, G Griffiths, (eds.), 'Acoustical Oceanography', Proc. Institute of Acoustics Vol. 23 Part 2, 2001.

where k_r is the horizontal wavenumber component and J_0 is the Bessel function of the first kind of order zero. The Green function g satisfies the wave equation,

$$\left[\frac{\partial^2}{\partial z^2}+k^2(z)-k_r^2\right]g(z,z_0;\gamma)=-2\delta(z-z_0) \tag{4}$$

3. Asymmetry of the Iso-Speed Shallow Water Sound Field

In a horizontally stratified, range independent iso-speed shallow water waveguide, the Green function solution to Equation (4) for a receiver *below* the source $z \le z_0$ is given by [6],

$$g(z,z_0,\gamma)=\frac{e^{-i\gamma(z_0-z)}\left(1+R(\gamma)e^{-i2\gamma z}\right)\left(1+S(\gamma)e^{-i2\gamma(H-z_0)}\right)}{\gamma\left(1-S(\gamma)R(\gamma)e^{-i2\gamma H}\right)},\quad z\le z_0. \tag{5}$$

Equation (5) may be decomposed into a continuum of upward and downward traveling plane wave components with amplitude weighting functions $a^+(z_0,\gamma)$ and $a^-(z_0,\gamma)$ respectively,

$$g(z,z_0,\gamma)=(1/\gamma)\left[a^-(z_0,\gamma)e^{i\gamma z}+a^+(z_0,\gamma)e^{-i\gamma z}\right]. \tag{6}$$

Comparison of Equations (5) and (6) gives explicit expressions for the weighting functions as,

$$\left.\begin{aligned}a^-(z_0,\gamma)&=a(z_0,\gamma)\\ a^+(z_0,\gamma)&=R(\gamma)a(z_0,\gamma)\end{aligned}\right\},\quad \text{where}\quad a(z_0,\gamma)=\frac{e^{-i\gamma z_0}+S(\gamma)e^{-i2\gamma(H-z_0)}}{1-S(\gamma)R(\gamma)e^{-i2\gamma H}}. \tag{7, 8}$$

Combining Equations (2) and (6), and neglecting the contribution to the field from evanescent, inhomogeneous waves for which $k_r > \omega/c$, where k is the free-space wavenumber ω/c, and c is the sound speed in water, the acoustic pressure may be expressed in the form,

$$p(r,z)=\int_0^k (1/\gamma)\left[a^-(z_0,\gamma)e^{i\gamma z}+a^+(z_0,\gamma)e^{-i\gamma z}\right]J_0(k_r r)\,k_r\,dk_r \tag{9}$$

Making use of Equation (7) and the change of variable $\gamma=\left(k^2-k_r^2\right)^{1/2}$, Equation (9) becomes

$$p(r,z)=\int_0^k a(z_0,\gamma)\left[e^{i\gamma z}+R(\gamma)e^{-i\gamma z}\right]J_0(k_r r)\,d\gamma,\qquad z\le z_0 \tag{10}$$

Except for the exclusion of inhomogeneous waves, Equation (10) is exact for iso-speed waveguides. The form of Equation (10) makes explicit the exact asymmetry of the vertical wave amplitude spectrum with respect to the seabottom plane wave reflection coefficient, namely; $a^+(z_0,\gamma)/a^-(z_0,\gamma)=R(\gamma)$. Equation (10) describes the acoustic field produced by a point source. The principle of linear superposition ensures that this vertical asymmetry is preserved even for sources of arbitrary geometry and directionality. The only restriction is that the entire source distribution is closer than the receiver to the sea surface. Expressing the acoustic field as the sum of an integral over all upward traveling plane waves and an integral over downward traveling plane waves generalizes Equation (10) to arbitrary source distributions, thus,

$$p=\int\left[dp^+(\gamma)+dp^-(\gamma)\right],\quad \frac{dp^+(\gamma)}{dp^-(\gamma)}=e^{-2i\gamma z}R(\gamma) \tag{11}$$

For each wave arriving from above there is a corresponding wave from below with the only difference being a single reflection from the seabed $R(\gamma)$ and a change of phase $e^{-2i\gamma z}$ resulting from the additional propagation delay.

4. Measurement Principle

The beamformed output $P(r,\gamma)$ from a Vertical Line Array (VLA) of N sensors, at range r, in the direction $\theta = \sin^{-1}(\gamma/k)$ to the horizontal axis is calculated from

$$P(r,\gamma)=\sum_{n=1}^{N} p(r,z_n)b_n e^{-i\gamma z_n}, \tag{12}$$

where z_n denotes the depth of the n^{th} hydrophone and b_n amplitude shading coefficients. Combining Equations (10) and (12) yields,

$$P(r,\gamma)=\int_0^k a(z_0,\gamma')J_0(k_r'r)[\psi(\gamma-\gamma')+R(\gamma')\psi(\gamma+\gamma')]d\gamma', \quad z_n \le z_0 \tag{13}$$

where $\psi(\gamma\pm\gamma')=\sum_{n=1}^{N} b_n e^{-i(\gamma\pm\gamma')z_n}$ is the un-normalised directivity of the array as a function of vertical wavenumber component $\gamma'=(k^2-k_r'^2)^{1/2}$. For a uniform, un-shaded array $b_n = 1$, with vertical separation distance Δz, $z_n = z_1 + (N-1)\Delta z$,

$$\psi(u)=e^{iu\bar{z}}\frac{\sin(uL/2)}{\sin(u\Delta z/2)}, \tag{14}$$

Here L is the array length $L = N\Delta z$, and $\bar{z} = z_1 + L/2$ is the depth of its acoustical centre. Beam steer directions above the horizontal $\gamma > 0$, attenuate through sidelobe rejection waves arriving from below. Similarly, beams steered below the horizontal, $\gamma < 0$, suppress waves from above. When the variation in the reflection coefficient is small over the angular beamwidth of the main beam, the ratio between the measured beam responses when steered at equal angles above and below the horizontal may provide an acceptable estimate for the complex plane wave reflection coefficient $R(\gamma)$. A difficulty with this technique is that wave components arrive at the array centre coherently whose sum exhibits oscillatory behavior that is entirely an artifact of the measurement principle. The resulting directivity measurement for the coherent wavefield, as shown in Section 5, is in generally poor agreement with the exact value. A scheme is now proposed by which the importance of the phase relationship between waves is substantially diminished, leading to an improved directivity estimate that is sufficiently accurate for bottom loss measurement.

4.1 Incoherent waves; a necessary condition for accurate directivity measurements

From Equation (13), the beam power $B(r,\gamma)=|P(r,\gamma)|^2$ may be expressed as,

$$B(r,\gamma)=\int_0^k\int_0^k\{a(z_0,\gamma')a^*(z_0,\gamma'')[\psi(\gamma-\gamma')+R(\gamma')\psi(\gamma+\gamma')]\,[\psi^*(\gamma-\gamma'')+R^*(\gamma'')\psi^*(\gamma+\gamma'')]J_0(k_r'r)J_0(k_r''r)\}d\gamma'd\gamma'' \tag{15}$$

Weighting the beam power by the source-receiver range r, and integrating over all r remove the interference terms in this expression due to coherent waves of the same propagation angle. A range integrated beam response function $\bar{B}$ is now defined by,

$$\bar{B}(\gamma)=\int_0^\infty B(r,\gamma)\,r dr. \tag{16}$$

The practical implementation of Equation (16) involves recording the signals at the sensors of a VLA receiver while the source is simultaneously towed away from, or towards, it (Figure 1).

Applying Equation (16) to (15) and eliminating the cross terms $k_r' \neq k_r''$ by virtue of the orthogonality identity,

$$\int_0^\infty J_0(k_r'r)J_0(k_r''r)\,r dr = \delta(k_r'-k_r'')/k_r' \tag{17}$$

leads to the simplification of Equation (15) as,

$$\bar{B}(\gamma)=\int_0^k k_r'^{-1}|a(z_0,\gamma')|^2|\psi(\gamma-\gamma')+R(\gamma')\psi(\gamma+\gamma')|^2 d\gamma', \qquad |a(z_0,\gamma)|^2=\frac{1+\cos(\gamma(2H-z_0))}{1+\mathrm{Re}\{R(\gamma)e^{-2i\gamma H}\}}. \tag{18, 19}$$

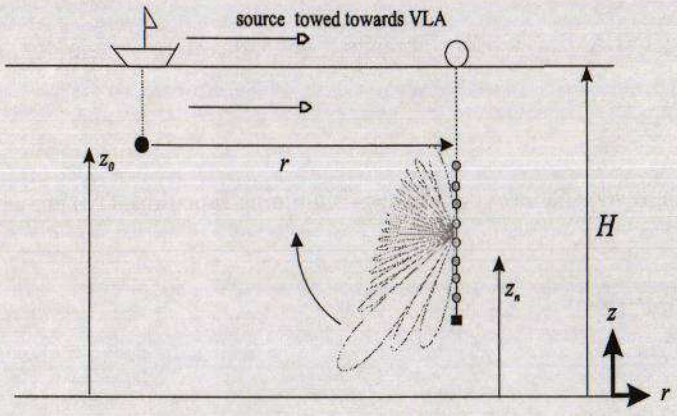

Figure 1. Schematic diagram of a procedure for the measurement of bottom loss and reflection phase of the seabed in an iso-speed, shallow water waveguide.

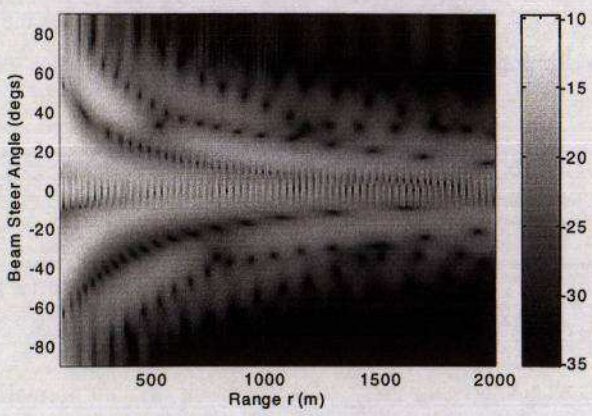

Figure 2. Beam power response function (dB Re arbitrary units) versus beam steer angle and source range computed from Equation (20) based on the parameters listed in Table 1a and b.

The result of performing the integration over r is that interference now only occurs between waves with propagation angles that are symmetrical about the horizontal. All other wave components are summed incoherently. In practice, the measurements will be confined to some maximum range r_{max} which sets a fundamental limit on the correlation length equal to $\Delta k_r = 2\pi / r_{max}$. Wave components whose horizontal wavenumber component differ by more than Δk_r may be regarded as uncorrelated. It is therefore anticipated that values of r_{max} greater than a few kilometers is sufficient for current purposes. For moderate length arrays, waves arriving from below, not too close to broadside, can be neglected when a beam is steered above the horizontal, and vice-versa for beams steered below the horizontal. The expression for $\overline{B}$ therefore closely approximates to,

$$\overline{B}(\gamma) \approx \int_{-k}^{k} |A(z_0,\gamma')|^2 \Psi(\gamma-\gamma') d\gamma' , \qquad -k \le \gamma \le k , \tag{20}$$

where, $|A|^2 = k_r^{-1}|a|^2$, for $\gamma \ge 0$, and $|A|^2 = k_r^{-1}|a|^2|R|^2$, for $\gamma \le 0$, and $\Psi = |\psi|^2$. The form of Equation (20) is that of a completely uncorrelated wave field as is often assumed in ambient noise modeling. Noting that k_r and Ψ are both even functions of γ, any asymmetry in the measured function $\overline{B}$ about the horizontal $\gamma = 0$ is therefore entirely due to a single additional interaction with the seabottom. For sufficiently long arrays therefore,

$$\frac{\overline{B}(-\gamma)}{\overline{B}(\gamma)} \approx \frac{\left|a^+(z_0,\gamma)\right|^2}{\left|a^-(z_0,\gamma)\right|^2} = |R(\gamma)|^2 . \tag{21}$$

In the hypothetical limit of $L/\lambda \to \infty$, as the beamwidth tends to zero and sidelobe rejection becomes increasingly perfect, the dependence of the sound field on the source depth and range, and the surface reflection coefficient becomes progressively weaker. The measurement procedure is therefore insensitive to these parameters for realistic length arrays. It is therefore not necessary to keep the source at a fixed known depth whilst being towed from the receiver, but only that it remains above the receiver.

5. Bottom Loss Measurement - A Numerical Example

The measurement principles discussed in Section 4 are now illustrated by the results from computer simulations of an iso-speed shallow water waveguide overlaying a homogenous elastic half space. Table 1 lists the parameters used in the simulations. These were chosen arbitrarily and are representative of a fairly low loss bottom with a critical angle of about 35° (Figure 5). Losses at the seabed are by conversion of the incident sound into shear waves, and by visco-thermal losses which are introduced by means of complex wave speeds.

Waveguide parameters			Receiver parameters		Source parameters	
H (m)	Density (kgm^{-3})	c (m/s)	z_1 (m)	N, L (m)	z_0 (m)	f (Hz)
200	1000	1500	190	21, 120	190	100

Table 1a. Parameters of waveguide, source and receiver

Compressional wave speed (m/s)	Shear wave speed (m/s)	Density (kgm^{-3})
1850-50i	350-10i	1500

Table 1b. Seabottom Parameters

The acoustic pressure at each of the sensors of a 21 element VLA was computed from the application of Equation (2) to Equation (5) with the upper limit of integration truncated to k thereby limiting the computer prediction to the propagating waves. The plane wave reflection coefficient R of the seabed appearing in Equation (5) was computed from the Rayleigh formula for sound transmission across a fluid-solid plane interface. The reflectivity at the sea surface was assumed to take the constant value $S(\gamma) = -0.999$. Integration was performed using a high precision adaptive integration routine. The acoustic pressure predictions were then beamformed using Equation (12), and the process repeated for many values of the source range between 100 m and 2km.

From Figure 2, the beam response with increasing source range decays faster at high angles to the axis compared with that close to the axis. It is therefore reasonable to assume that the reflection loss at the seabed is greatest closest to normal incidence. However, the variations in beam power are highly oscillatory resulting from the interference between modes. For this reason the asymmetry property predicted by Equation (11) is obscured in these measurements. Figure 3 suggests that the directivity measurement is poorly conditioned and that it may not be possible to obtain accurate information about the reflection loss at the seabed. In order to establish more clearly whether this directivity measurement is sufficiently accurate for determining $|R|$, a comparison between the measured vertical directivity at r = 1 km (dashed line), and the theoretical variation based on Equations (7) and (8) (solid line) is presented in Figure 4 below.

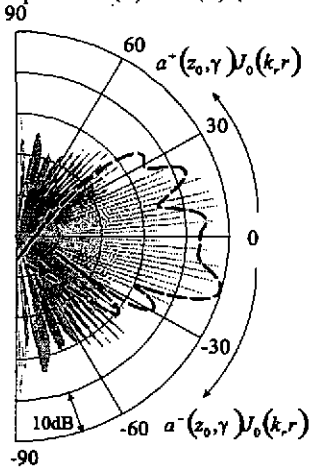

Figure 3. Comparison between the theoretical vertical directivity (solid curve), calculated from Equations (7, 8), and the 'measured' directivity by a 21 element VLA receiver 1km from the source (dashed curve).

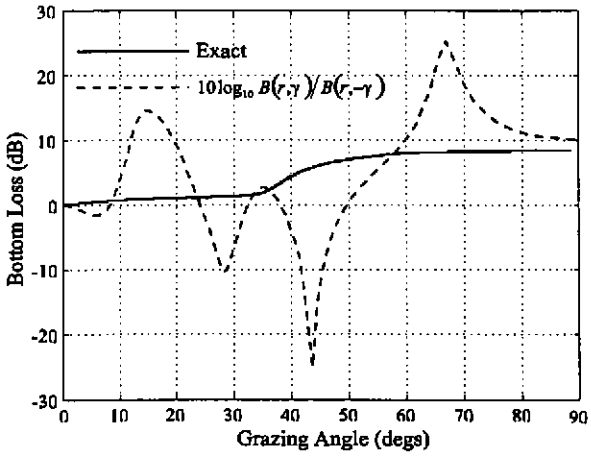

Figure 4. Comparison between the exact bottom loss and that derived from the ratio of beam intensity response functions measured at a range of 1km from the source.

In this example, the theoretical directivity is dominated by twelve discrete modes that interact with the seabed at angles less than the 35° critical angle (Figure 3). Since the mode shape functions are simply residues of the theoretical Green function of Equation (5), they too must posses at their eigenfrequencies the vertical asymmetry indicated by Equation (11). Above the critical angle, the directivity falls off sharply. At these high angles the directivity is characterized by the continuous portion of the Green function wavenumber spectrum [1] whose magnitude is greatly diminished compared to the modes present below the critical angle. The measured directivity at r = 1 km plotted in Figure 4 appears to follow the general behavior of the directivity function. However, the corresponding bottom loss estimate derived from the ratio of measurements $10\log_{10}[B(r,\gamma)/B(r,-\gamma)]$, plotted in Figure 4 (dashed line), is in poor agreement with the exact value (solid line). Much between agreement is obtained from $10\log_{10}\overline{B}(\gamma)/\overline{B}(-\gamma)$ plotted in Figure 5 below.

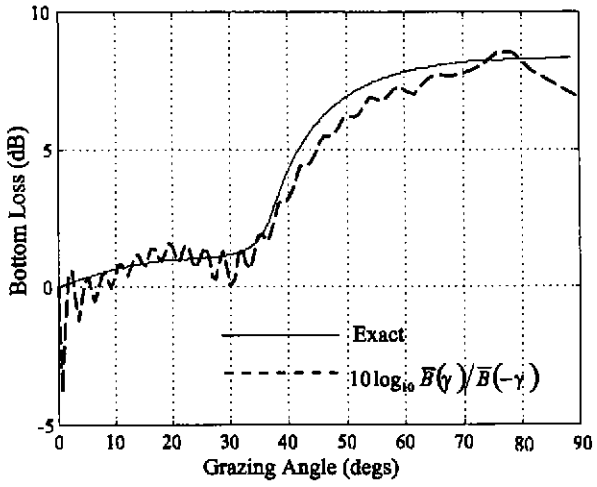

Figure 5. Comparison between the exact bottom loss and that derived from Equations (20) and (21).

Apart from non-physical oscillations in the 'measured' bottom loss measurement arising from the presence of sidelobes in the array directivity, agreement is generally good, with typical error being less than 1dB.

6. Matched Field Inversion in Beam Space for the Measurement of Reflection Phase

A technique is now proposed that permits the measurement of the reflection phase $\tan^{-1}(\mathrm{Im}\,R(\gamma)/\mathrm{Re}\,R(\gamma))$. The discussion in Section 5 has demonstrated that this is not possible from direct FFT beamforming measurements in a coherent wavefield, and an alternative scheme for making this measurement is now presented. The approach has two advantages over previous methods. First is that it can be used to determine the reflection phase at one angle at a time, independently of its value external to the main beam. Second, the reflection phase may be determined independently of the bottom loss. The proposed measurement technique is based upon principles of matched field inversion (MFI). A conventional implementation of MFI applied to the current problem would involve trying to determine the reflection phase at the seabed at all incidence angles simultaneously. By having to adjust separately the complex reflection coefficients in a reasonable discretization of the incidence angles between 0° and 90° the calculation is computationally intensive. Furthermore, measurement error at any one angle, for example, due to poor signal to noise ratio, may corrupt the inversion results at the other angles. The matched field inversion in this case is said to be poorly conditioned. The approach described here overcomes this fundamental difficulty. The measurement of the reflection phase in the direction of the beam steer angle $\theta = \sin^{-1}(\gamma/k)$ is obtained by finding the value that maximizes the function $\bar{C}$. This function is defined below in Equations (22) and (23) as the range weighted correlation function between the measured beam formed output as a function of range $P(r,\gamma)$, and a computer prediction $\hat{P}(r,\gamma,\hat{\phi})$ based on the assumed reflection phase $\hat{\phi}$. By analogy with the definition of $\bar{B}$ in Equation (16), $\bar{C}$ is defined by,

$$\bar{C}(\gamma,\hat{\phi}) = \int_0^\infty C(r,\gamma,\hat{\phi})\, r\, dr\,, \qquad C(r,\gamma,\hat{\phi}) = P(r,\gamma)\hat{P}^*(r,\gamma,\hat{\phi}), \tag{22, 23}$$

Equations (22) and (23) represent a modified linear (or Bartlett) correlator over source range in beam space. The replica beamformed output $\hat{P}$ by the VLA is calculated from an identical expression to the exact result of Equation (13), but which includes two essential approximations. They are that (*i*), only waves entering the main beam of the array, $\gamma-\Delta\gamma \le \gamma \le \gamma+\Delta\gamma$, are included and that (*ii*), the reflection phase over this band of angles is taken to be constant. The replica beam response for beam steer directions below the horizontal, where $\gamma < 0$, is therefore computed from,

$$\hat{P}(r,\gamma,\hat{\phi}) = \hat{R}\int_{\gamma-\Delta\gamma}^{\gamma+\Delta\gamma} \hat{a}(z_0,\gamma',\hat{\phi})J_0(k'_r r)\Psi(\gamma+\gamma')d\gamma',\ \gamma \le 0\,, \qquad \hat{a}(z_0,\gamma,\hat{\phi}) = \frac{e^{-i\gamma z_0} + S(\gamma)e^{-i2\gamma(H-z_0)}}{1 - S(\gamma)|\hat{R}|e^{i\hat{\phi}}e^{-i2\gamma H}} \tag{24, 25}$$

and $\Delta\gamma = \pi/L$, denoting the approximate half-width of the main beam. A similar expression to Equation (24) applies for beam steer directions above the horizontal with $\Psi(\gamma-\gamma')$ replacing $\Psi(\gamma+\gamma')$, and the factor $\hat{R}$ absent. Our first attempt at the inversion will assume a replica wave amplitude function $\hat{a}(z_0,\gamma,\hat{\phi})$ with $|\hat{R}|$ determined exactly. In this case the only

remaining unknown quantity is the reflection phase at the beam steer angle of interest. Its optimum value can be obtained by scanning between 0° and 180° and selecting the value that maximizes $\overline{C}$. However, it will be shown that the technique is insensitive to the assumed value of $|\hat{R}|$, and that the phase may be determined with equal accuracy by assuming an arbitrary constant value of $|\hat{R}|$ close to unity (but not equal to it since $a(\gamma)$ may become singular at the modal eigen-frequencies). A clearer understanding of the factors that determine the behavior of Equations (22) and (23), and the reasons why $\overline{C}$ is insensitive to $|\hat{R}|$, follows by substituting Equations (13) and (24) into these equations to give,

$$\overline{C}(\gamma,\hat{\phi}) = \hat{R}^* \int_0^k \int_{\gamma-\Delta\gamma}^{\gamma+\Delta\gamma} a(z_0,\gamma'')\hat{a}^*(z_0,\gamma',\hat{\phi})[\psi(\gamma-\gamma'') + R(\gamma'')\psi(\gamma+\gamma'')]\psi^*(\gamma+\gamma')\left[\int_0^\infty J_0(k_r'r)J_0(k_r''r)rdr\right]d\gamma' d\gamma'', \quad \gamma \le 0 \tag{26}$$

Substitution of the term in large square brackets by the Dirac delta function using the orthogonality relationship of Equation (17), and performing the integration over γ'' leads to the simpler equation,

$$\overline{C}(\gamma,\hat{\phi}) = \hat{R}^* \int_{\gamma-\Delta\gamma}^{\gamma+\Delta\gamma} k_r'^{-1} a(z_0,\gamma')\hat{a}^*(z_0,\gamma',\hat{\phi})[\psi(\gamma-\gamma') + R(\gamma')(\gamma+\gamma')]\psi^*(\gamma+\gamma')d\gamma', \quad \gamma \le 0 \tag{27}$$

Following the integration over range, the correlation between waves of different propagation angles is set equal to zero. Furthermore, since the replica wavenumber spectrum is only defined in the main beam $\gamma-\Delta\gamma \le \gamma' \le \gamma+\Delta\gamma$, and equals zero outside it, evaluation of the correlation is confined to this relatively narrow bandwidth. By assuming that for steer directions below the horizontal waves arriving from above can be neglected, Equation (27) simplifies further to,

$$\overline{C}(\gamma,\hat{\phi}) \approx \hat{R}^* \int_{\gamma-\Delta\gamma}^{\gamma+\Delta\gamma} k_r'^{-1} R(\gamma')a(z_0,\gamma')\hat{a}^*(z_0,\gamma',\hat{\phi})\Psi(\gamma+\gamma')d\gamma', \quad \gamma \le 0 \tag{28}$$

Numerical simulations have shown that the approximations implicit in Equation (28) incur insignificant error over the exact expression of Equation (27). The simplified expression of Equation (28) has a straightforward interpretation as the integral taken over the main beam, of the product of the physical wave amplitude spectrum $a(z_0,\gamma)$ and its computer prediction $\hat{a}(z_0,\gamma,\hat{\phi})$, amplified by k_r^{-1}, and smoothed by the beam power response function Ψ. For beam steer angles less than the critical angle, an incorrect choice of reflection phase causes the modal peaks in a and $\hat{a}$ to occur at different wavenumbers. The product $a(z_0,\gamma')\hat{a}^*(z_0,\gamma',\hat{\phi})$ is consequently small despite broadening of the spectral peaks in these amplitude functions following convolution by the array response function. When the assumed reflection phase agrees with that at the seabed, however, the modal peaks are coincident leading to a much larger value for $\overline{C}$. At beam steer angles above the critical angle, however, the correlation function is computed from the product of two continuous functions of wavenumber. Its sensitivity to changes in reflection phase is therefore much poorer than when the directivity functions are characterized by discrete modal wavenumber components. The inversion is therefore anticipated to be far less effective above the critical angle, than below it. It now remains to be shown whether a replica field based on the two, quite significant, simplifying approximations (*i*) and (*ii*) above is in sufficiently good agreement with the measured response when evaluated at the exact reflection phase to permit its use in matched field inversion. Furthermore, to establish whether the correlation function has sufficient sensitivity to error in the reflection phase to enable its optimum value to be located with adequate resolution.

7. Determination of Reflection Phase - A Numerical Example

Figure 6 depicts the typical variation in the magnitude of the correlation function as a function of the assumed reflection phase between 0° and 180° for the three array lengths L/λ = 5, 10 and 20. In this example, the beam steer direction is 11.5° below the horizontal with half wavelength separation distance between the sensors.

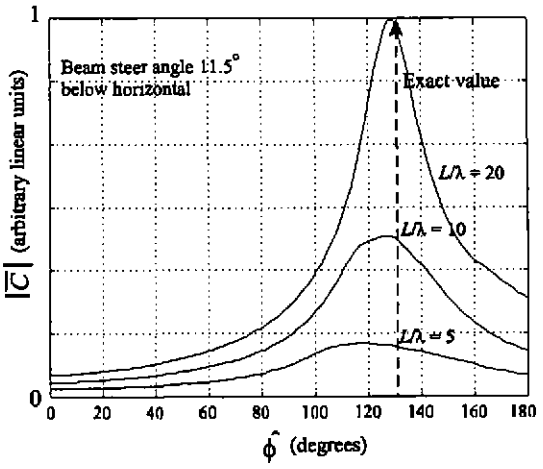

Figure 6. Variation of the correlation function between 'measured' beam former output and a replica field versus trial reflection phase

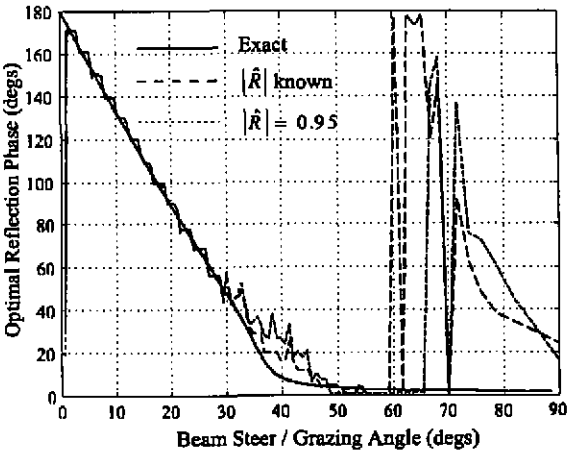

Figure 7. Variation of optimal reflection phase versus beam steer angle

All three curves exhibit a distinct peak close to the exact reflection phase of 130°, with the error decreasing with increasing array length. Numerical simulations have shown that the width of the peaks, indicating the sensitivity to reflection phase mismatch, becomes broader with increasing beam width, and the bandwidths of both the physical and assumed modal peaks (i.e., increased modal damping). Except for very long arrays with beamwidths less than the widths of the modal peaks, the finite array resolution is the factor that dominates the sensitivity of the correlation function to reflection phase mismatch. However, even the shortest array in this example is shown to yield the correct reflection phase to better than 10° accuracy. The successful matched field inversion depicted in Figure 6 is achieved unconventionally in the sense that no normalisation of the computed replica function has been performed. This is because its magnitude is principally determined by the reflection loss, and this remains approximately constant as the reflection phase is being surveyed. In principle, normalisation of the replica field should enable this approach for the determination of reflection phase to be extended to include reflection loss. However, the sensitivity of the correlation function to this quantity is anticipated to be weak, particular at low frequencies when there may be only one, or even no modes, arriving at the main beam.

Figure 7 above presents a comparison between the variation of the optimum reflection phase with beam steer angle, and the exact reflection phase as a function of grazing angle. The vertical array used in this example comprises of 21 sensors separated by a distance of 0.5λ. The dashed curve corresponds to the results obtained with a replica field computed using the exact reflection loss $|R(\gamma)|$, while the dotted curve is the optimal reflection phase obtained by assuming the constant value of $|\hat{R}| = 0.95$ at all beam steer angles. Agreement in both cases is better than 5° at beam steer angles below the 35° critical angle, but degrades significantly at angles above this. Beyond 60° very little agreement is observed. Agreement in Figure 7 between the two reflection phase estimates with the exact value confirms the validity of the technique even when knowledge of the reflection loss is unavailable. The cause of erroneous results at angles exceeding the critical angle is revealed by the behavior of $a(z_0, \gamma)$ at these angles. In this wavenumber range the spectrum is continuous unlike that below the critical angle where it is dominated by discrete modal peaks. A function derived from the product of two wide bandwidth signals, is itself a wide bandwidth signal. The integral of such a quantity, particularly following convolution by the array response function, is therefore insensitive to changes in field dependent quantities such as the reflection phase. Consequently, the determination of reflection phase above the critical angle is occasionally ambiguous; the accuracy of the technique in this case is therefore unreliable. Fortunately, the interaction of sound at angles greater than the critical angle are quickly attenuated and do not propagate to long range. Knowledge of reflection phase at these angles is therefore unnecessary for predicting long range sound transmission.

8. Conclusions

Two techniques have been described. One is for the measurement of the magnitude of the plane wave reflection of an iso-speed shallow water channel, and the other for the measurement of the reflection phase. Both techniques use measurements of the beamformed output by a receiver VLA as a function of source range. Furthermore, the two techniques may be implemented independently, i.e., the first technique does not require knowledge of the reflection phase, and the second technique may be implemented independently of bottom loss information.

Acknowledgments

The author gratefully acknowledges the funding of this work by DERA Winfrith.

References

[1] Schmidt H and Jensen FB. Evaluation of experimental techniques for determining the plane wave reflection coefficient at the sea floor, in Ocean seismo-acoustics, T Akay and M Berkson (eds.), NATO Conference series, Series IV: Marine Sciences. (1986).

[2] Frisk GV, Oppenheim AV and Martinez DR. A technique for measuring the plane wave reflection coefficient of the ocean bottom. *Journal of the Acoustical Society of America*1980; **68**: 602 - 612.

[3] Lambert M and Lesselier D. On the retrieval of the plane wave reflection coefficient of a seabed in shallow water. *Acta acustica* 1995; **3**: 243 - 249.

[4] Cox. BT and Joseph P. A comparison of Hankel Transform Algorithms' Performance for Use in Shallow Water Applications, in *Proceedings of the 16th International Congress on Acoustics and 135th Meeting Acoustical Society of America,* Seattle, 1998, Vol III, 1639 - 1640 (1998).

[5] Yang TC and Yates TW. Acoustic inversion of bottom reflectivity and bottom sound speed profile. *Journal of Oceanic Engineering*. 1996; **21**: 367 - 376.

[6] Frisk G.V. Ocean and seabed acoustics. Prentice Hall, Inc., 1994.